Coalescence of Designed and Natural Space Radiological Environments

Tyler R. Steiner¹, Jarvis A. Caffrey², and Jonathan D. Barth³

¹ NASA Glenn Research Center, Cleveland, OH ² NASA Marshall Space Flight Center, Huntsville, AL

³ NASA Goddard Space Flight Center, Greenbelt, MD

Primary Author Contact Information: tyler.r.steiner@nasa.gov

[Placeholder for Digital Object Identifier (DOI) to be added by ANS]

There are many differences and few similarities across various radiological environments in space – both natural and induced. The caveats and nuances of such environmental comparisons must be appreciated for fair assessments. Comparing different environments enables a deeper understanding of what makes each environment unique as well as the identification of any overlapping technological areas. The radiological environments discussed pertain to proposed missions and/or designs. These include radioisotope power systems, fission surface power, nuclear electric propulsion, nuclear thermal propulsion, the Lunar surface, the Martian surface, Earth's orbits, and the Jovian radiation belt.

I. INTRODUCTION

With renewed and continued interest in nuclear technology for space applications, the consideration of radiological environments cannot be neglected. There are ongoing efforts to develop a number of nuclear technologies. Radioisotope power systems (RPS) can supply electrical power output ranging from tens of watts to hundreds of watts. Fission surface power (FSP) intends to supply kilowatts for crewed Lunar, then Martian habitats. Nuclear electric propulsion (NEP) and nuclear thermal propulsion (NTP) seek to provide kilowatts to megawatts of electrical and thermal power, respectively, to reduce transit times in space.

Contained in this document is a collection of designed nuclear systems for space. Each design presented was developed for a larger system. The requirements, scopes, goals, etc. will vary from system to system, but the information collected is tied to a completed system design.

In addition to the induced radiation environments, there are natural radiation environments in space. This document will coalesce the natural radiation environments on the Lunar surface, Martian surface, low Earth orbit (LEO), medium Earth orbit (MEO), geosynchronous Earth orbit (GEO), and the Jovian radiation belts.

The caveats and radiation exposure associated with each environment will elucidate the differences and similarities between environments – and can be used to identify areas of overlap, or lack thereof.

II. RADIATION ENVIRONMENTS OF DESIGNED SYSTEMS

Throughout the recent decades there have been many systems designed, and less recently, hardware tested for space-nuclear missions. Minimizing the radiation exposure to crew, electronics, and other hardware are driving factors in the designs. Minimizing radiation exposure often comes at the cost of increased mass. The exposure levels herein are associated with completed designs or tests. Radiological exposure to humans from nuclear technologies is required to be less than 2 rem per mission year set by NASA-STD-3001 [1].

II.A. Radioisotope Power Systems

The historical choice of fuel for a NASA radioisotope power system has been PuO_2 , with the majority of the plutonium being ^{238}Pu . Neutrons can be produced from PuO_2 fuel via four mechanisms: spontaneous fission, induced fission, (α ,n) reactions with low Z isotopes, and photoneutron formation [2]. The neutron activity of PuO_2 containing 81% ^{238}Pu is around 11,300 n/s/g [3].

The gamma dose associated with ²³⁸Pu is high intensity, but easily shielded. The gamma dose of unshielded ²³⁸Pu is roughly 4.4 krad/hr/g at 1 cm. The gamma dose of ²³⁸Pu shielded by 0.08 cm thick tantalum is roughly 44 mrad/hr/g at 1 cm. Daughters of ²³⁸Pu cause a minor increase in the intensity of gamma-rays over time. After 5 years, the daughters increase the unshielded dose by 7 rad/hr/g and increase the shielded dose by 73 mrad/hr/g [3].

PuO₂ has been flown on several space missions in radioisotope thermoelectric generators (RTG). RTGs use PuO₂ in the form of general purpose heat sources (GPHS). The dose from 8 3-year-old GPHS fuel sources for the Multi-Mission Radioisotope Thermoelectric Generator (MMRTG) is shown in Fig. 1. [4] Fig. 1 compares the measured dose to a modeling tool – RPS-DET [4].

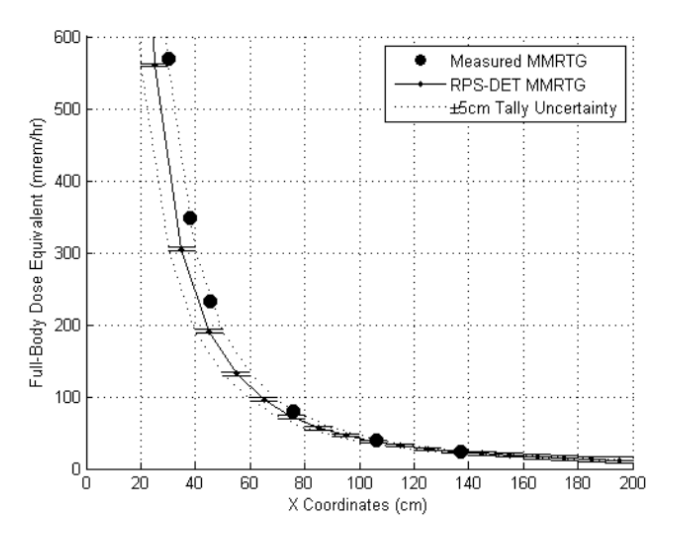


Fig. 1. MMRTG dose compared to RPS-DET model [4].

The MMRTG offers nonzero shielding, which should be considered when comparing the dose from the MMRTG against bare PuO_2 and other nuclear environments. The dose-attenuating materials of the MMRTG are shown in Fig. 2. The MMRTG is capable of producing 2000 W_{th} and 110 W_e at beginning of mission [5].

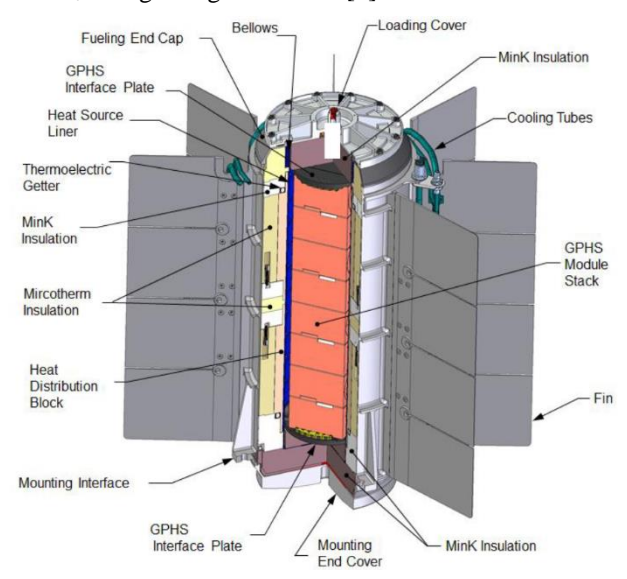


Fig. 2. MMRTG [5].

II.B. Kilowatt Reactor Using Stirling TechnologY

The Kilowatt Reactor Using Stirling TechnologY (KRUSTY) was a prototype of a 5 kW_{th}, 1 kW_e fission reactor [6]. KRUSTY was constructed with highly enriched uranium fuel and operated for 28 hours. KRUSTY primarily used stainless steel (SS) shielding. [6] SS shielding will shield gammas more effectively than neutrons. At roughly 1 m from the core, the fast neutron flux was 1E9 n/cm²/s and the gamma dose rate was 200 rad(Si)/hr [7].

The KRUSTY reactor configuration is shown in Fig.

Heat pipe (Ha230/Na) (SS, B₄C, SS) Upper Ref.(BeO) Neutron Source Shim Ref. (BeO) (at max height) Cast Fuel (U7.5Mo) Radial Ref. (BeO) Radial Shield(SS) Lower Ref. (BeO) B4C Stack (at max height) Bottom of Vacuum Vessel (SS) Lower Shield (SS, B4C, SS) Comet Platen (AI) (1.5" short of full insertion) Comet Table (AI)

Fig. 3. KRUSTY reactor configuration [6].

II.C. Fission Surface Power

3.

Concepts for fission surface power (FSP) have been explored for decades. A 40 kW_e design was developed in 2010 that selected highly enriched UO₂ fuel pins, Stirling convertor power conversion, and to bury the reactor in a 2 m deep excavation. This 186 kW_{th} design carried requirements of: 8 years of operation, 5 Mrad gamma dose (Si) outside of the shield, and a neutron fluence of 2.5E14 n/cm² outside of the shield [8]. Converting the gamma dose and neutron fluence to dose rate and neutron flux – assuming constant levels over 8 years – these requirements become 20 mrad/s and 10E5 n/cm²/s. The shielding and dimensions of this concept are shown in Fig. 4.

Following the above study, in 2011, the radiation limits for power conversion systems were adjusted from 5 Mrad and $2.5E14 \text{ n/cm}^2$ to 10 Mrad and $5E14\text{ n/cm}^2$ [9].

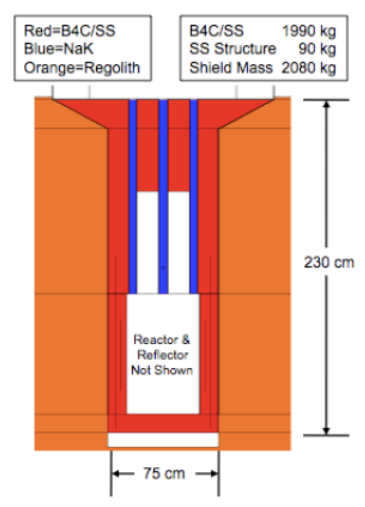


Fig. 4. 2010 FSP buried shield configuration [8].

II.D. System for Nuclear Auxiliary Power 10A

System for Nuclear Auxiliary Power (SNAP) 10A is the only fission reactor power system launched by the United States. The highly enriched uranium reactor was launched in 1965, produced 34 kW_{th}, and 500 W_e. The reactor used a 100 kg, roughly 50 cm diameter, and 70 cm tall LiH shield [10]. The shield was designed to limit the total radiation 533 cm from the core to about 4E4 krad/y (1.2 rad/s) and 5E12 n/cm²/y (1.6E5 n/cm²/s) [10]. The reactor was intended to operate for 1 year, but was shut down after 43 successful days.

II.E. Nuclear Electric Propulsion

Comprehensive overviews of both NEP and NTP systems are available in the National Academies report [11]. For NEP, rate-based effects that are dominant in NTP (including gamma/neutron heating) are less dominant in the radiation mitigation design, though still not to be neglected. Instead, total accumulated ionizing dose and non-ionizing dose (TID and TNID, respectively) are the primary hazards to be avoided.

For the purposes of the comparison in this paper, two relevant published examples of NEP systems are discussed, although many such studies have been pursued to support mission architecture planning and system sizing. NEP systems often require shielding mass that approaches or rivals the mass of the reactor itself, and significant focus has been historically applied to the sizing and optimization of shielding systems, including the RSMASS and its derivatives from Sandia National Laboratories [12].

The Jupiter Icey Moons Orbiter (JIMO) was intended to be the first flight project within the Prometheus Project. This was a broad government project on the design of a NEP system, largely intended for outer planet scientific payloads. It went through a design cycle that evolved from ~135 kWe (500 kWth) up to 200 kWe (1000 kWth) and

would power both the thrusters and the spacecraft [13]. With the Jovian trapped radiation environment as its intended destination, the intense trapped electron flux provides an additional set of requirements for extensive shielding or other radiation mitigations of sensitive hardware in the payload. These two environments, nuclear reactor radiation and natural trapped radiation, and their associated mitigations were largely handled separately and by separate organizations. This is especially evidenced by review of the JIMO Final Report which describes the challenging natural radiation design while scarcely mentioning the existence of reactor radiation but still imposes multiple tons of shielding at the payload due to natural environments [14]. Meanwhile, survey of the reactor shielding code evaluation report which in large part handled the reactor radiation with an implied target dose and flux value at a payload region assumed 50 meters away [15]. Note that the scope of the referenced KAPL reactor shielding paper does not specifically claim that this is a finalized design, but rather intended to assess the viability of different codes to evaluate representative designs which are described in the paper. Recently, researchers in China have revisited this design and have presented an optimization approach that shows some alternative design approaches with claims of modest mass improvements for similar dose targets by 'floating' a tungsten slab of reduced diameter within a large LiH body, in addition to Be, B4C, and SS316 applied in various layer configurations. Neutron 1 MeV-equivalent flux is approximately 9E9 n/cm² and 215 krad(Si) at a payload location 50 m from 'top' of core, operated for 15 years. Unshielded, that same location encounters 2.9E16 n/cm² and 1800 krad(Si) [16].

An NEP system for Mars human transport was evaluated in a COMPASS study, and assumed to operate at

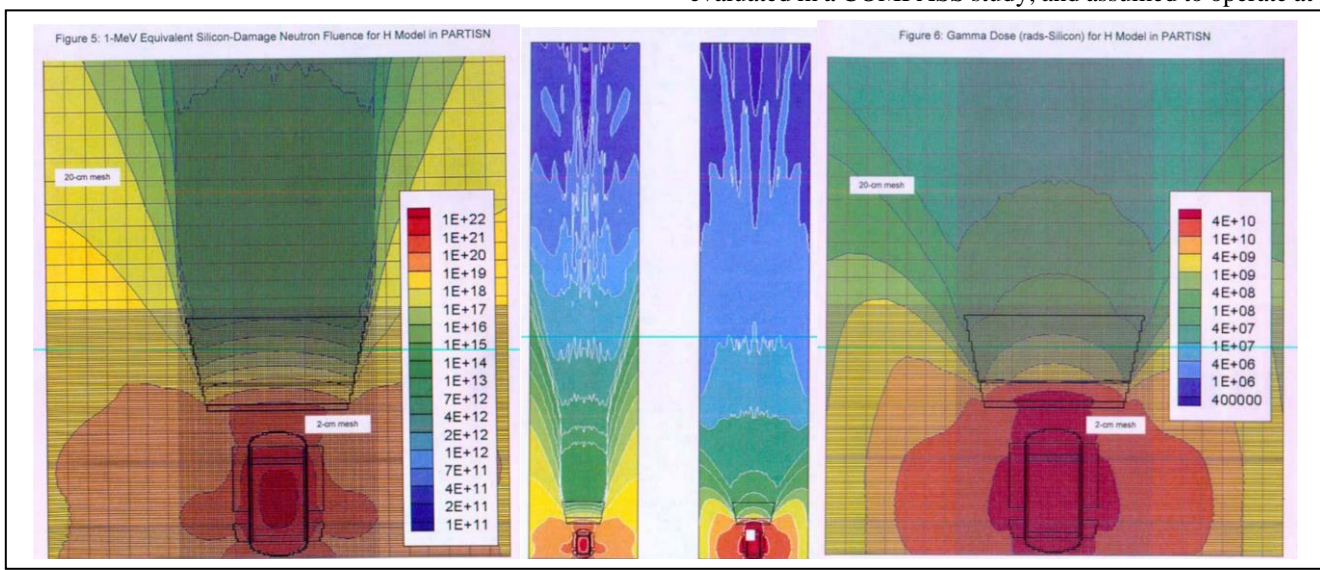


Fig. 5. Neutron fluence profile (1MeV equivalent - left), and gamma TID profile (rad(Si) – right) for JIMO as shown in the KAPL code evaluation study [15]. Center shows the same plot with an 18 meter extent. Other size details are available in the cited literature.

much higher power levels and thrusts than the smaller scale development and science payload applications assumed for JIMO or other demonstration systems. Those higher power levels are assumed necessary for viable human exploration applications, but the radiation and shielding challenges grow alongside that increase in power. The radiation evaluation in the COMPASS study assumed a reactor operating continuously at 10 MWth for 2 years. Dose limits described here target 25 krad to the Brayton cycle hardware located adjacent to the reactor and shield, 100 Mrad to the power management and distribution (PMAD) hardware located 50 meters away (boom separated), and limits dose to the first wall of the crew compartment area target 50 rem/vr (100 rem total). It does not account for any knockdowns of dose afforded by mass in the crew habitat. A significant trade study of shield mass, geometry, and reactor design choices is well described in the cited report [17].

II.F. Nuclear Thermal Propulsion

NTP systems operate at significantly higher power levels and reject as much thermal energy as possible directly to a working fluid, which is directed out of a nozzle to generate thrust. The operations thus result in relatively short burns, on the order of minutes or hours, with long quiescent periods to 'coast' between thrust operations. Additionally, their use in vehicle architectures that assume extremely large volumes of liquid hydrogen (or other hydrogenous propellants) means that the observed dose to payload or crew is encountered in a very different manner.

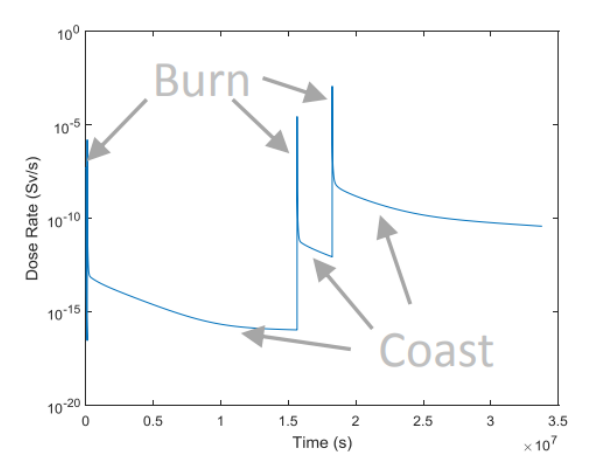


Fig. 6 Intense spikes of dose at crew habitat are delivered intermittently through a mission using NTP, with increasing doses received as propellant is expended. Y axis is log-scale but not normalized to any specific application or power level. Provided for relative visual context only [18].

The ROVER/NERVA program yielded a wealth of historical engineering design and testing data for this type of technology, although only a small fraction is available in public digitally accessible literature. As with Shielding

mass was allocated such that the total accumulated doses to crew were less than 5 Rem/yr (50 mSv/yr), which is still consistent with US federal annual radiation worker limits under normal conditions, although does not necessarily meet the most recent NASA standards for dose from nuclear technology [1]. This value was assumed to be accumulated positioned approximately 100 meters away and protected largely by the presence of a diminishing mass of liquid hydrogen in the propellant tank. The specifics of these mission architectures varied. With respect to the NERVA engine design, being a single engine of 75,000 lbf thrust and ~1.5 GWth power level, reference missions revisited in the early 1990's assumed short-stay, opposition class architectures [19], [20].

Closer to the reactor, radiation dose profiles for NERVA are not accessible in public literature, however some component values are referenced and suggest 50 Mrad TID gamma dose and 2E16 cm⁻² fast neutron fluence (>1 MeV) [21]. That same reference also describes the significant gamma heating that poses an additional, and in many cases more challenging, hazard to nuclear propulsion systems.

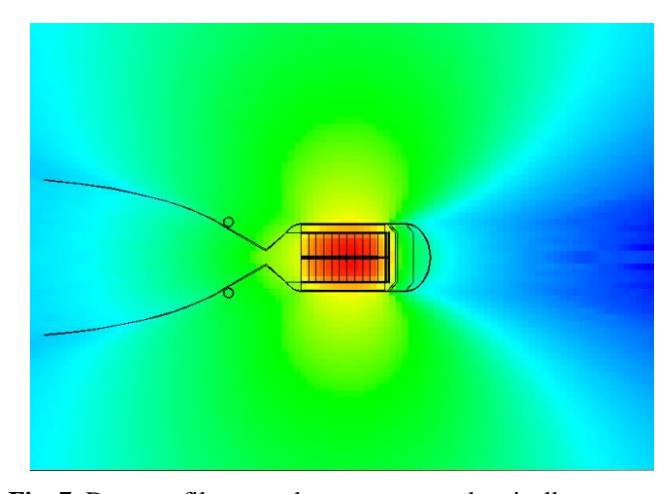


Fig. 7. Dose profiles near the reactor vary drastically, especially compared to conical shadow-shielded region [18].

More recent studies of nuclear thermal propulsion tend to assume smaller thrust requirements (with multiple engines) with proportionally smaller power levels and thus lower radiation dose rates/fluxes, since longer burn times or engine clustering introduces other radiation challenges to the system. A more significant deviation that often does help radiation design is the shift towards lower enrichment and more thermalized neutron spectra, which can considerably reduce leakage fraction of neutrons for equal power levels. As shield mass allocations then shift toward reactor and reflector mass, and secondary absorption and emission of gamma radiation does not track alongside the change in neutron emission characteristics.

The Design Reference Architecture Mars mission (DRA 5.0) baselined 3x 25 klbf, each with 1500-2430 kg of shielding assumed, though significant optimization was assumed to be available, and a cursory revisit in 2017 indicated ~1400 kg shield per engine would satisfy a 5 rem mission dose limit, and did not account for additional shielding afforded by supplies or consumables in the habitat. Significant additional optimization is assumed to be available but requires further development of high fidelity deep-penetration shielding models, establishment of intermediate hardware dose requirements, and radiation-informed crew habitation design, all of which are ongoing work.

III. NATURAL RADIATION ENVIRONMENTS

The space radiation environment of our solar system can be thought of in three ways: (1) the solar process: how radiation is produced by the Sun, how solar wind and solar particle events manifest; (2) galactic cosmic rays (GCR), highly energetic extra-solar particles; and (3) planetary radiation belts, how radiation from the Sun and GCR are captured by planetary magnetic fields to produce concentrated regions of energetic particles.

Solar flares are bursts of electromagnetic radiation, which travel at the speed of light and reach the Earth in about 8 minutes. They can contain microwave, visible light, ultraviolet, and gamma radiation, which can cause disruptions to Earth satellites and blackouts that may last from minutes to hours and is harmful to astronauts. Coronal Mass Ejections (CME) are immense clouds of plasma, as much as 10¹⁷g of material, which erupt from the chromosphere, containing electrons, protons, and heavy ions [22]. The protons and heavy ions can be collectively referred to as Solar Energetic Particles (SEP) and can have energies up to 1 MeV/nucleon. CME travel slower than solar flares, reaching Earth on a time scale of several hours to several days, and dealing significant damage or harm to spacecraft subsystem electronics and humans alike.

Solar flares and CME are not well correlated but can occur together in the cases of large events. While both phenomena are not explicitly predictable, the general level of solar activity is well understood to trend with respect to an 11-year "solar cycle", although this number may vary from 9 to 13 years. The periodicity of the solar cycle, which sees peaks and ebbs in regularity solar flares and CME can be described as having a 4-year solar minimum phase and a 7-year solar maximum phase [22].

The sun's corona also continuously emits "solar wind", a stream of protons, alpha particles, and a small amount of heavy ions, as well as electrons that balance the difference of positively charged particles. The magnitude of particle density and composition also vary over the solar cycle and is impacted by solar flares and CME.

The energy of solar wind ions is typically 0.5 to 2.0 keV/nucleon, and density is between 1 to 10 particles/cm³. This low energy plasma does not present a significant

threat to spacecraft or humans, as it is readily shielded by thin materials, however, cumulative exposure over time can damage materials on the outside of spacecraft, such as solar cells [23].

Galactic Cosmic Rays (GCR) are highly energetic particles originating from outside the solar system. They are commonly attributed to formation from the remnants of supernova, objects interacting with supermassive black holes, magnetized neutron stars, or galactic collisions. GCRs are isotropic, can consist of any element on the periodic table, from hydrogen to uranium, and have energies ranging from keV/nucleon to GeV/nucleon, although there is no theoretical limit to how energetic they could be. Table I shows the relative compositions of both Solar Wind of GCR [22].

Table I. Comparison of Solar Wind Particles and GCR [22].

	Relative abundance	
Particle Type	Solar Wind	Galactic Cosmic Rays
Protons (H ⁺)	95%	83%
Alpha Particles (He ⁺²)	4%	13%
Other Heavy ions	1%	1%
Electrons	Number needed to make solar wind neutral	3%

When GCR interact with matter, they typically produce a large number of secondary particles, such as electrons, protons, neutrons, and other heavy ions through spallation. While the total dose deposition from GCR is relatively low, 10 rad/yr in minimally shielded silicon, the effective dose to humans can be severe due the higher relative biological effective dose attributed to heavy ions and the secondary particles produced in their interactions [22].

Given the varying mass and energy of particles that makeup both SEP and GCR, it is useful to present the full spectrum in terms of Linear Energy Transfer (LET), which allows us to examine the impact of energetic particles on a single spectrum and draw conclusions about LET of particles to their relative biological effectiveness or impact on sensitive electronics. Fig. 8 presents the interplanetary flux of particles/cm²/s with respect to LET for both GCR during Solar Max and Solar Min and for the SEP averaged over the peak 5 minutes, worst day, and worst week of a CME. The reference event for this CME is the October 1989 event, one of the largest events in recorded history, is often used as a "99% worst case" environment. While the SEP can be understood "worst case", GCR should be understood as the local background during any mission. The presented resultant flux is transmitted through 100 mils of aluminum, with silicon selected as the device material.

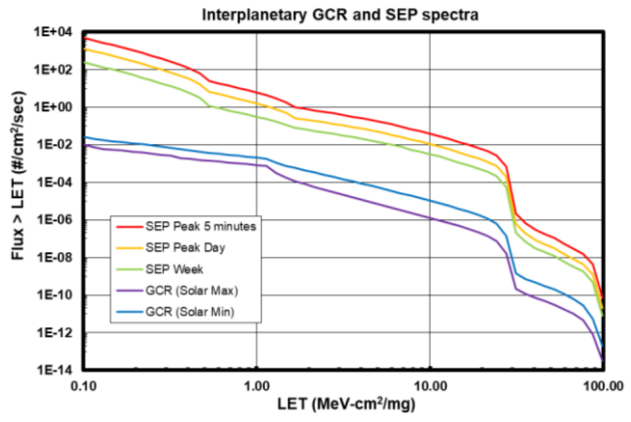


Fig. 8. Interplanetary flux of particles and LET.

Planetary radiation belts are defined by the interaction of planetary magnetosphere and solar and galactic cosmic rays. Charged particles either from solar wind or GCR become trapped in the magnetic fields, forming radiation belts.

In the absence of the solar wind, Earth's magnetic field would appear entirely symmetrical, with poles at magnetic north and south, and extending several Earth radii into space. The solar wind pushes in on the magnetosphere, causing it to buckle on the dayside of the Earth, and elongate on the nightside, with the full tail extending several hundred Earth radii. Fig. 9 shows the Earth's magnetic field lines condensing and elongating in the solar wind [24].

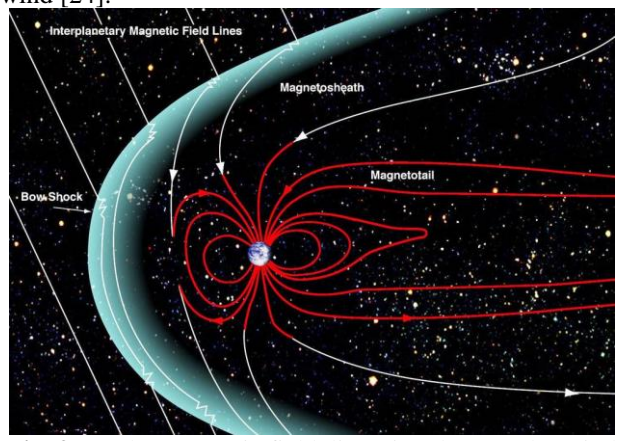


Fig. 9. Earth's magnetic field distortion due to solar wind [24].

The Earth's Van Allen radiation belts are bound by its fluctuating magnetosphere and are comprised of relativistic protons, electrons, and heavy ions. There are generally considered to be two belts, an inner and outer belt [25]. The inner radiation belt altitude has a radius of 0.2 to 2 Earth Radii, (~1000km to 12000 km) has a high population of energetic protons, although electron populations are generally less than 1 MeV. Due to the offset of magnetic and geometric poles, the inner radiation belt is responsible for the South Atlantic Anomaly (SAA), a region over of

South America and the Atlantic Ocean with proportionally highly elevated levels of charged particles. The outer radiation belt extends from 3 to 10 Earth Radii (13,000 to 60,000 km), and is comprised of highly energetic electrons, as well as a lesser population of protons and heavy ions. While both radiation belts can vary with solar events, the outer belt can be significantly impacted by high levels of solar wind and CME. Extremely powerful CME have also been known to create temporary short-lived radiation belts between the traditional inner and outer belts [25], [26].

Various dose environments have been modelled and can be compared. Fluence environments were modelled from ESA's SPace ENVironment Information System (SPENVIS) for SEP and the Jovian radiation belts and the International Radiation Environment Near Earth (IRENE) for Earth radiation belts. Dose was calculated inside solid aluminum spheres in the FASTRAD modelling software, although SHIELDDOSE-2 was used for the Jovian dose. All environments have been modelled at 95% confidence during solar maximum and normalized to annual dose. Dose is reported inside silicon, with at 100 mils (2.54 mm) of aluminum shielding. Figure 10 displays the dose-depth curve in silicon for 95% confidence over various radiation environments. Please note that these dose-depth curves should only be considered estimates only, and only prescriptive for the specific orbit or environment.

NASA document SLS-SPEC-159 Cross-program design for specification for natural environments (DSNE) further describes the natural space radiation environment [27].

III.A. Lunar Surface

The radiation on the lunar surface environment will look very similar to interplanetary, excepting that lunar surface functions to block half of the dose, acting as a 2pi shield. Secondary particle generation will also occur in the lunar regolith, resulting in the creation of additional neutrons, protons, electrons, and heavy ions due to interaction with SEP and GCR. Lunar surface dose is 2.17 krad (Si) annually.

III.B. Martian Surface

The radiation of the Martian surface, while extreme compared to the surface of the Earth, is relatively benign with respect to most planetary surface environments. The majority of SEP will be attenuated by the Martian atmosphere. As such, the majority of dose comes from GCR and secondary particles. Without any shielding, dose on the Martian surface is estimated to be 7.6 rad (Si) annually during solar minimum. Additional shielding of high energy GCR by aluminum and other high-Z material will tend to cause buildup of neutrons and other secondary particles, resulting in an even higher dose [28], [29].

III.C. Earth Orbit

LEO missions generally tend to stay below the inner radiation belt, avoiding most of the trapped particle radiation. Even so, missions that routinely pass through the SAA or have an inclination that will take them over the poles will have an increased exposure. LEO mission dose is usually composed of high energy trapped protons, trapped electrons, and solar protons (if a polar mission). Two LEO missions were considered. The first mission is a circular orbit at 550 km with 6° inclination (relatively similar environment to the ISS orbit, which is at 56.1°). The second mission is at 800 km circular orbit with a 98° (polar) inclination. Doses respectively are 2.47 krad (Si) and 5.57 krad (Si) annually.

Geosynchronous orbits will match the rotational period of the Earth, wherein they will return their exact position in the sky every day. Geostationary orbits are a special type of this orbit, having an inclination of 0°, such that objects will remain at a fixed point to ground-based observers. GEO orbits are parked solidly in the outer radiation belt, and receive an extreme amount of radiation dose from highly energetic electrons. A geostationary orbit was considered, with the circular orbit of 35,793 km. Dose for this mission is 259 krad (Si) annually.

MEO missions generally stay between LEO and GEO missions, but their orbits can be circular or high eccentric. Missions will make several passes per day through the inner and outer radiation belts, being exposed to both

highly energetic protons and electrons alike. The considered MEO mission is highly eccentric, with an apogee and perigee of 30,000 and 300km, and a 20° inclination. Dose for this mission is 1,195 krad (Si) annually.

III.D. Jovian Radiation Belts

The total radiation dose of a spacecraft executing a 20 hour Europa flyby with a 5 mm thick aluminum shield is roughly 10⁴ rad(Si) – with the TID dominated by trapped electrons in Jupiter's magnetosphere [30]. Ref [30] also provides TID as a function of aluminum thickness for the same environmental conditions.

The annual mission dose of a Jovian Europa orbit is shown in Fig. 10 along with other natural environments.

IV. CONCLUSIONS

The radiological nature of induced and natural environments in space varies in flux, species, energy, and dose. There are substantial differences across space radiological environments – some of which are nuanced. The radiation environment of space applications cannot be generalized. Each activity will require unique considerations.

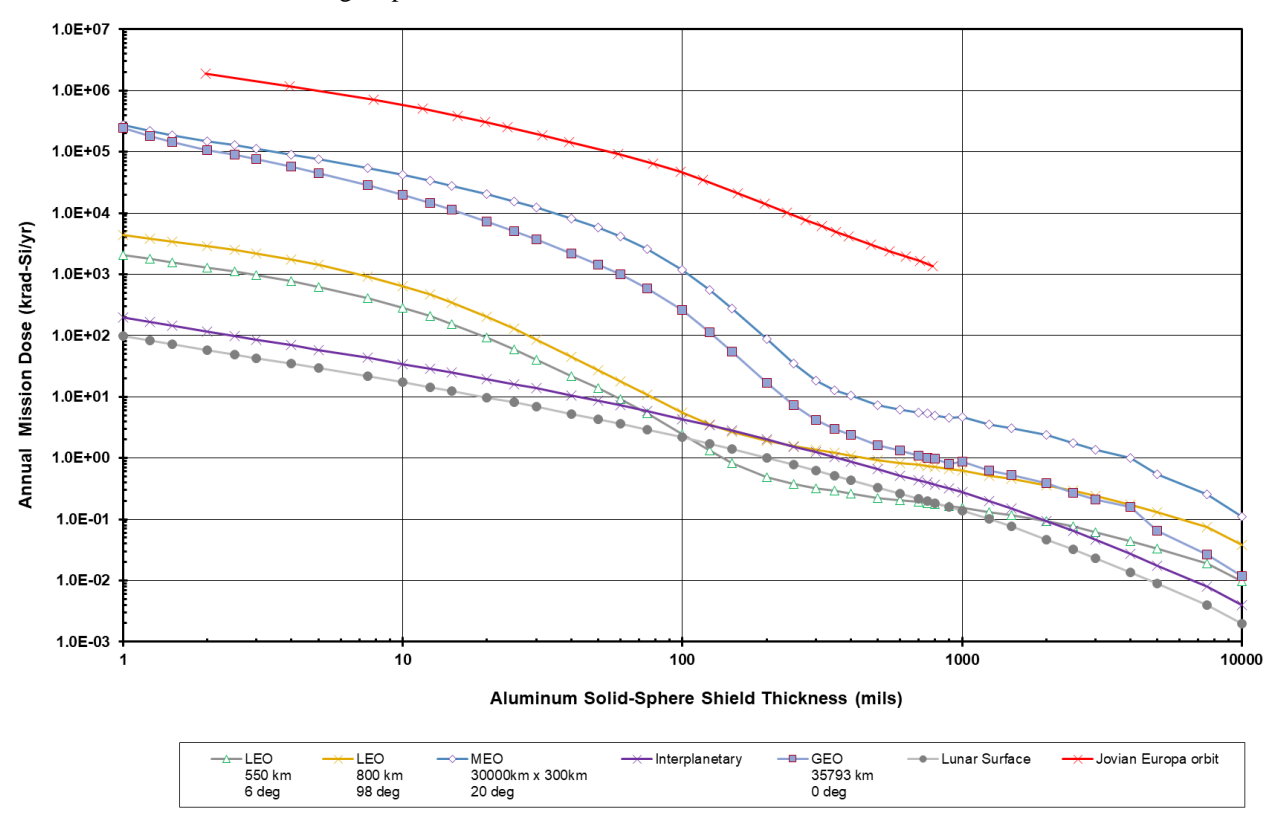


Fig. 10. Dose depth curve in silicon with 95% confidence.

REFERENCES

- [1] NASA Office of the Chief Health and Medical Officer, "NASA-STD-3001 NASA SPACEFLIGHT HUMAN-SYSTEM STANDARD VOLUME 2: HUMAN FACTORS, HABITABILITY, AND ENVIRONMENTAL HEALTH REVISION D," 2023.
- [2] M. Taherzadeh, "Technical Report 3201555 Neutron Radiation Characteristics of Plutonium Dioxide Fuel," NASA, 1972.
- [3] G. M. Matlack and C. F. Metz, "LA-3696 Radiation Characteristics of Plutonium-238," Los Alamos Scientific Laboratory, 1967.
- [4] M. B. Smith, "Radioisotope Power Source Dose Estimation Tool," in *IEEE Aerospace Conference*, 2018.
- [5] D.J. Clayton, J. Bignell, C.A. Jones, et al., "SAND2013-10589 Nuclear Risk Assessment for the Mars 2020 Mission Environmental Impact Statement," Sandia National Laboratories, 2014.
- [6] D. Poston, M. Gibson, T. Godfroy and P. McClure, "KRUSTY Reactor Design," *Nuclear Technology*, vol. 206, 2020.
- [7] D. Poston, Private Communication: 2024-10-09 Email.
- [8] L. Mason, D. Poston, et al., "NASA TM-2010-216772 Fission Surface Power System Initial Concept Definition," 2012.
- [9] C. Bowman, E. Shin, O. Mireles, R. Radel and A. Qualls, "Radiation Specifications for Fission Power Conversion Component Materials. NASA/TM-2011-216996," NASA, 2011.
- [10] S. Voss, "AFWL-TN-84-14 SNAP REACTOR OVERVIEW," Air Force Weapons Laboratory, 1984.
- [11] National Academies of Sciences, Engineering, and Medicine, "Space Nuclear Propulsion for Human Mars Exploration," The National Academies Press, 2021.
- [12] A. Marshall, "RSMASS-D Models: An Improved Method for Estimating Reactor and Shield Mass for Space Reactor Applications," Sandia National Laboratories, 1997.
- [13] S. Voss, "Nuclear Security Considerations for Space Nuclear Power: A Review of Past Programs with Recommendations for Future Criteria," *Nuclear Technology*, vol. 206, 2020.
- [14] NASA Jet Propulsion Laboratory, "Prometheus Project Final Report No. 982-R120461," 2005.
- [15] J. Stephens, T. Miller and M. Zerkle, "SPP-67210-0009 Summary of Prometheus Radiation Shielding Nuclear Design Analysis," Knolls Atomic Power Laboratory, 2006.
- [16] J. Baihui, et al., "Mass Optimization of Shielding Materials for 100 kWe-level Space Nuclear Reactor," *Atomic Energy Science and Technology*, vol. 67, 2024.
- [17] L. Mason, S. Oleson, D. Jacobson, P. Schmitz, L. Qualls, M. Smith, B. Ade and J. Navarro, "NASA-TM-20210016968 Nuclear Power Concepts and Development Strategies for High-Power Electric Propulsion Missions to Mars," 2022.
- [18] J. Caffrey and M. Rodriguez, "NASA-TM-20180002053 Integrated NTP Vehicle Radiation Design," in *Nuclear and Emerging Technologies for Space*, 2018.
- [19] J. Clark, P. McDaniel, S. Howe and I. Helms, "NASA-TM-105711 Nuclear Thermal Propulsion Technology: Results of an Interagency Panel," 1993.
- [20] S. Borowski, "NASA-TM-19920001873 Nuclear Thermal Rocket Workshop Reference System - ROVER/NERVA," 1992.
- [21] J. Mayer, D. Robinson and R. Wyre, "NASA-TN-D-5347 NERVA Control Drum Actuator Irradiation Test Program," 1969.
- [22] J. Barth, "Modelling Space Radiation Environments," IEEE NSREC Short Course, 1997.

- [23] K. Ogilvie and M. Coplan, "NASA-TM-19950015967 Solar Wind Composition," 1995.
- [24] A. Kaase, "Earth's Magnetosphere," NASA GSFC, 2011.
- [25] W. Li and M. Hudson, "Allen radiation belts: From discovery to the Van Allen Probes era," *Geophysical Research: Space Physics*, vol. 124, 2019.
- [26] N. Ganushkina, I. Dandouras, Y. Shprits and j. Cao, "Locations of boundaries of outer and inner radiation belts as observed by Cluster and Double Star," *Geophysical Research: Space Physics*, vol. 116, 2011.
- [27] NASA, "SLS-SPEC-159 Cross-program design for specification for natural environments." 2021.
- [28] Hassler, et al., "Mars' Surface Radiation Environment Measured with the Mars Science Laboratory's Curiosity Rover," *Science*, vol. 343, 2104.
- [29] D. Matthia and T. Berger, "The radiation environment on the surface of Mars - Numerical calculations of the galactic component with GEANT4/PLANETCOSMICS," *Life Sciences in Space Research*, vol. 14, 2017.
- [30] A. Goel, S. Krishnamoorthy, T. Swenson, et al., "Design for CubeSat-based dust and radiation studies at Europa," *Acta Astronautica*, vol. 136, 2017.
- [31] R.D. Lorenz, E.S. Clarke, "Influence of the Multi-Mission Radioisotope Thermoelectric Generator (MMRTG) on the local atmospheric environment," *Planetary and Space Science*, no. 193, 2020